International Journal of Thermophysics, Vol. 22, No. 5, September 2001 (© 2001)

Thermophysical Properties of Binary and Ternary Fluid Mixtures from Dynamic Light Scattering[1]

A. P. Fröba,[2] S. Will,[2,3] and A. Leipertz[2,4]

Several thermophysical properties of R507, a binary refrigerant mixture, and R404A, a ternary mixture, have been determined by dynamic light scattering (DLS), in both the liquid and the vapor states, along the saturation line approaching the vapor–liquid critical point. Data for the thermal diffusivity a and sound speed c_S cover a range of temperatures down to 270 K, and data for the surface tension σ and kinematic viscosity ν down to 230 K. For both mixtures the behavior of all properties determined can be correlated well by the mass-weighted sum of the respective pure component data, when all data are represented as a function of the reduced temperature.

KEY WORDS: binary mixture; dynamic light scattering; kinematic viscosity; R507; R404A; ternary mixture; thermal diffusivity; sound speed; surface tension.

1. INTRODUCTION

Dynamic light scattering (DLS) is an unique diagnostic tool for the determination of a variety of thermophysical properties of fluids using a basically identical experimental setup [1–4]. In pure fluids, the thermal diffusivity can be found from the linewidth of the Rayleigh component of the spectrum of scattered light which arises from entropy fluctuations [5–7]. In binary fluid mixtures, the thermal diffusivity and the mutual diffusivity can basically be

[1] Paper presented at the Fourteenth Symposium on Thermophysical Properties, June 25–30, 2000, Boulder, Colorado, U.S.A.

[2] Lehrstuhl für Technische Thermodynamik (LTT), Friedrich-Alexander-Universität Erlangen-Nürnberg, Am Weichselgarten 8, D-91058 Erlangen, Germany.

[3] Technische Thermodynamik/Wärme- und Stofftransport (TTWSt), Universität Bremen, FB4, Badgasteiner Straße 1, D-28359 Bremen, Germany.

[4] To whom correspondence should be addressed. E-mail: sek@ltt.uni-erlangen.de

0195-928X/01/0900-1349/0 © 2001 Plenum Publishing Corporation

determined simultaneously from the linewidth of the Rayleigh line, governed by microscopic fluctuations of temperature and concentration [8–10]. Additionally, for both pure fluids and fluid mixtures, information on sound speed and sound attenuation can be obtained from the Brillouin lines of the spectrum, which are shifted in frequency with respect to the incident light and which are caused by pressure fluctuations [4, 11–13]. Information on surface tension and kinematic viscosity can be derived from light scattering of surface waves, which are caused by the thermal movement of molecules resulting in so-called "ripplons" [4, 14]. For selected fluids, the dynamic viscosity can also be determined by seeding the liquid with small spherical particles of a known size [15], which sometimes is even possible simultaneously with other properties, e.g., with the mutual diffusion coefficient in binary liquid systems [16].

Apart from research proving the applicability of the measurement technique itself, investigations of fluid mixtures are quite rare and have—to the best of our knowledge—so far been restricted to binary mixtures [8–10, 17]. In the present paper, for the first time ternary mixtures have also been studied using the DLS technique. Measurements in the binary system R507 (50% wt. R125/50% wt. R143a) and in the ternary mixture R404A (44% wt. R125/52% wt. R143a/4% wt. R134a) were performed to study the behavior of saturated fluid mixtures when approaching the vapor–liquid critical point. For both the liquid and the vapor phases, the thermal diffusivity and sound speed were measured by light scattering from the bulk fluid, and liquid viscosity and surface tension were determined by surface light scattering.

Whether it is possible to determine signals simultaneously from concentration and temperature fluctuations is restricted mainly by the relative difference in the refraction indices of the mixture components and their concentration. However, for the fluid mixtures studied in this work the refractive indices of the pure components have comparable values [18–20] so that, from the Rayleigh component of scattered light, a signal from only temperature fluctuations associated with thermal diffusivity could be resolved.

2. METHOD AND EXPERIMENTAL SETUP

In contrast to conventional methods, most of which work with macroscopic gradients according to the desired quantities, DLS provides information on thermophysical properties of fluids in macroscopic thermodynamic equilibrium. The principle of the DLS techniques for the determination of these properties is given in some detail elsewhere (see, e.g., Refs. 1–4 and 21). In these investigations light scattering from bulk fluids

provides information on thermal diffusivity and sound speed, and light scattering from surface waves gives information on surface tension and kinematic viscosity.

The optical and electrooptical parts of the experimental setup used for the determination of sound velocity and thermal diffusivity are shown—from the top—in Fig. 1a. For performing light scattering from bulk fluids, the scattering volume, which is determined by the intersection of the incident beam and the axis of observation (dashed line), is located in the middle of the vessel. The principle of the scattering geometry which allows scattering by surface waves is shown schematically—from the front—in Fig. 1b. In this case, the detected scattering volume is located at the interface between the liquid and the vapor phases under saturation conditions. The only modification of the setup in Fig. 1a for the realization of surface light scattering experiments was to mount the pressure vessel in a vertical position.

As the light source, an argon ion laser ($\lambda_0 = 488$ nm) or an frequency-doubled continuous wave $Nd:YVO_4$-laser ($\lambda_0 = 532$ nm) was used. The laser power was up to 300 mW when working far away from the critical point and only a few milliwatts in the critical region. For determination of the sound speed, a reference beam shifted in frequency by an optoacoustic modulator was added to the scattered light. Scattered light was detected by two photomultiplier tubes (PMTs), and the cross-correlation function was calculated by a digital correlator. A more detailed description of the experimental setup is given in Ref. 4.

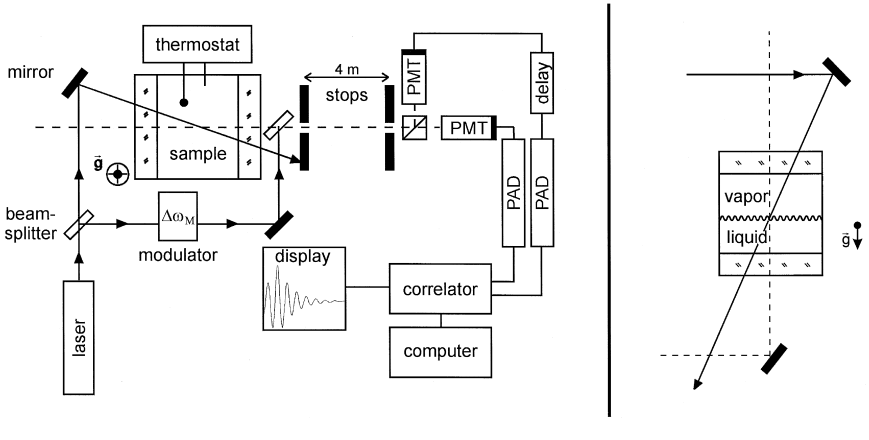

Fig. 1. Experimental setup. (a) Optical and electronic arrangement. (b) Scattering geometry: light scattering by surface waves.

According to the specifications of the manufacturer (Solvay), both refrigerant mixtures had a purity of $\geqslant 99.5\%$ and were used without further purification. The uncertainty in the composition for the binary mixture R507 is certified for each component within $\pm 1\%$ wt. For the ternary mixture R404A, the uncertainties in the composition are $\pm 2\%$ wt for R125, $\pm 1\%$ wt for R143a, and $\pm 2\%$ wt for R134a. For the present measurements, the samples were filled into a cylindrical pressure vessel (volume, $\approx 10\,\mathrm{cm}^3$) from the liquid phase to avoid decomposition, in particular, for the refrigerant R404A, which represents a near-azeotropic mixture.

The temperature of the pressure vessel, which is placed inside an insulated housing, is regulated through resistance heating and measured by calibrated 25- or 100-Ω platinum resistance probes with an uncertainty of ± 0.015 K. The temperature stability was better than ± 0.002 K during one experimental run. For each temperature point, typically six measurements at different angles of incidence were performed. For temperatures below room temperature, the insulating housing was cooled to about 10 K below the desired temperature in the sample cell by a lab thermostat.

3. RESULTS AND DISCUSSION

3.1. Binary Mixture R507

The experimental data for the thermal diffusivity and sound speed of R507 obtained by light scattering from bulk fluids are summarized in Tables I and II, respectively. The uncertainties of the measured mixture data can be estimated to be less than $\pm 1\%$ for the thermal diffusivity and less than $\pm 0.5\%$ for the sound speed. The thermal diffusivity, for both the vapor and the liquid phases, can be represented by the sum of a polynomial and an additionally necessary term which explicitly accounts for the critical behavior,

$$a = \left[\sum_{i=0}^{3} a_i \left(\frac{T}{\mathrm{K}} \right)^i + a_4 \left(1 - \frac{T}{T_\mathrm{C}} \right)^{0.67} \right] \cdot 10^{-8} \qquad (\mathrm{m}^2 \cdot \mathrm{s}^{-1}) \qquad (1)$$

where the critical temperature $T_\mathrm{C} = 344.06$ K was determined in our measurements by observation of the vanishing meniscus between the liquid and the vapor phases when approaching the critical point. For either phase the sound speed under saturation conditions may be described by a linear

correlation with an additional term to account for the curvature toward the critical point,

$$c_S = c_0 + c_1\left(\frac{T}{K}\right) + c_2\left(1 - \frac{T}{T_C}\right)^{\varphi} \qquad (m \cdot s^{-1}) \tag{2}$$

where φ represents an additional adjustable parameter. The coefficients for the data correlations determined from our experimental results by least-squares fits are listed for the thermal diffusivity and sound speed of R507 in Tables III and IV, respectively. The root-mean-square deviations of our values from the correlations and their ranges of validity are also listed. Each of these correlations represents the data within the experimental uncertainty.

In Figs. 2 and 3 the experimental results for the thermal diffusivity and sound speed of R507 are compared with a simple prediction method based on the properties of the pure components, respectively. In both figures the saturated vapor data are represented by the filled symbols and the saturated liquid data by open ones. Additionally, the pure-component data of R125 and of R143a are given by dotted and dashed lines, respectively.

Table I. Experimental Values of the Thermal Diffusivity a of R507 Under Saturation Conditions

Liquid phase		Vapor phase	
T (K)	a (10^{-8} m$^2 \cdot$ s^{-1})	T (K)	a (10^{-8} m$^2 \cdot$ s^{-1})
293.11	4.02	319.11	8.78
298.15	3.87	321.11	8.09
303.14	3.69	323.10	7.54
308.13	3.58	325.11	6.81
313.12	3.36	327.10	6.13
318.11	3.18	329.11	5.48
323.10	2.95	331.11	4.83
328.10	2.69	333.10	4.13
330.60	2.51	335.10	3.44
333.10	2.30	337.10	2.74
334.60	2.17	339.10	1.99
336.10	1.97	341.09	1.25
337.60	1.75	342.10	0.851
339.10	1.51	343.09	0.461
340.10	1.29		
341.10	1.06		
342.10	0.718		
342.60	0.551		
343.10	0.350		

Table II. Experimental Values of the Sound Speed c_s of R507 Under Saturation Conditions

Liquid phase		Vapor phase	
T (K)	c_s (m·s^{-1})	T (K)	c_s (m·s^{-1})
293.03	395.1	315.13	122.1
298.08	370.2	317.12	121.0
303.14	343.8	319.11	119.3
308.13	318.3	321.11	117.8
313.12	291.7	323.11	116.1
318.11	264.1	325.11	113.9
323.11	236.4	327.10	112.6
328.10	205.7	329.11	110.9
330.59	189.0	331.11	108.5
333.11	173.2	333.10	106.4
334.60	161.8	335.10	104.0
336.09	152.0	337.10	101.5
337.60	140.0	339.10	98.77
339.10	128.7	341.10	95.17
340.10	119.4	342.10	92.95
341.10	111.4	343.09	89.94
342.10	100.0		
342.60	95.13		

Table III. Coefficients of Eq. (1) for R507

	Liquid phase	Vapor phase
T range (K)	293–343	319–343
a_0	−245.3736	56.9995
a_1	2.1347466	−0.0372727
a_2	-7.197669×10^{-3}	-0.373374×10^{-3}
a_3	8.895267×10^{-6}	—
a_4	64.903	9.786
rms (%)	0.94	0.68

Table IV. Coefficients of Eq. (2) for R507

	Liquid phase	Vapor phase
T range (K)	293–343	315–343
c_0	817.13	159.409
c_1	−2.1687	−0.22293
c_2	741.24	102.317
φ	0.653	0.4550
rms (%)	0.29	0.14

The pure-component data for R125 were taken from former measurements [22]; those for R143a were measured in the course of this investigation and are reported separately [23]. The data are shown as a function of the reduced temperature,

$$T_R = T/T_C \tag{3}$$

To predict the mixture data on the basis of the pure-component data within the range investigated, we tried several approaches, e.g., using a simple weighting by the mass fractions or the mole fractions of the pure components. In all these cases, remarkable deviations appeared in the vicinity of the critical point when plotting the data against the temperature.

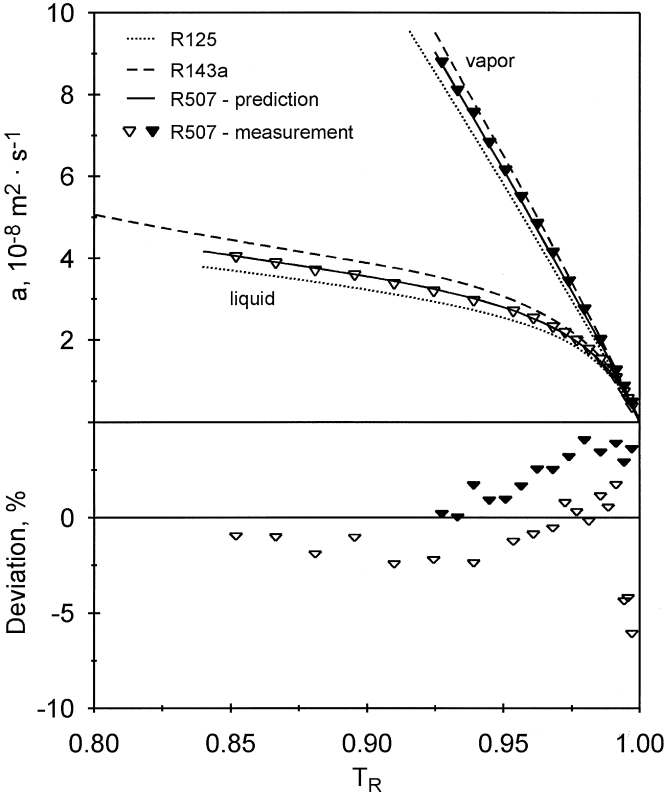

Fig. 2. Thermal diffusivity of the liquid (▽) and vapor (▼) phases under saturation conditions for the binary mixture R507 as a function of the reduced temperature in comparison to predictions (——) based on properties for the pure components R125 (·····) and R143a (– –).

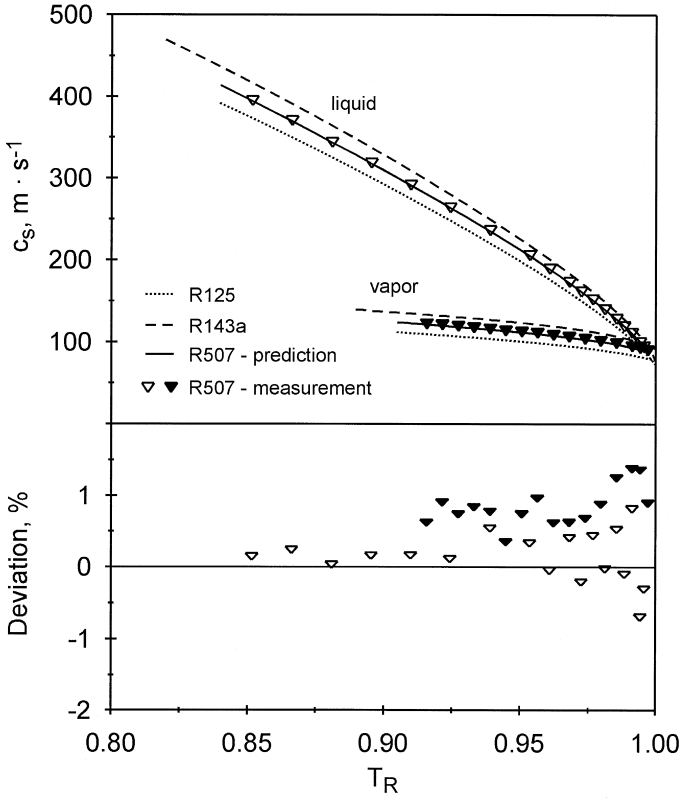

Fig. 3. Sound speed of the liquid (▽) and vapor (▼) phases under saturation conditions for the binary mixture R507 as a function of the reduced temperature in comparison to predictions (——) based on properties for the pure components R125 (·····) and R143a (– –).

However, using the reduced temperature as shown in Figs. 2 and 3, excellent agreement was found between the measured data and the predicted values when weighting with the mass fractions as indicated in the figures by the drawn line. The agreement was not this good when using the mole fractions. The data of the drawn line have thus been calculated, e.g., for the thermal diffusivity a_M of the mixture, according to

$$a_M(T_R) = \sum_j w_j a_j(T_R) \tag{4}$$

where w_j and a_j are the mass fraction and thermal diffusivity at the reduced temperature T_R of component j, respectively. For the sound speed the same

Table V. Viscosity and Surface Tension of R507 Under Saturation Conditions [a]

T (K)	$\tilde{\nu}$ ($mm^2 \cdot s^{-1}$)	η'' ($\mu Pa \cdot s$)	ρ' ($kg \cdot m^{-3}$)	ρ'' ($kg \cdot m^{-3}$)	ν' ($mm^2 \cdot s^{-1}$)	σ ($mN \cdot m^{-1}$)
243.15	0.2141	9.8	1271	11	0.2083	11.25
253.15	0.1939	10.2	1235	16	0.1882	9.90
263.15	0.1773	10.7	1199	23	0.1718	8.53
273.15	0.1609	11.2	1161	32	0.1557	7.22
283.15	0.1470	11.7	1122	44	0.1424	5.97
293.15	0.1347	12.2	1080	59	0.1308	4.74
303.15	0.1221	12.9	1034	79	0.1190	3.57
313.15	0.1100	13.7	981	106	0.1079	2.47
323.15	0.0963	14.9	917	145	0.0953	1.46
333.15	0.0793	16.8	827	206	0.0787	0.58

[a] Directly measured values for $\tilde{\nu}$ were combined with literature data for η'' from Ref. 27 and for ρ' and ρ'' from Ref. 26 to derive ν'. These density values were also used for the evaluation of σ.

procedure has been used. As can be seen from the deviation plots in Figs. 2 and 3, the prediction is very good, with deviations of less than 1.5% for the sound speed mixture data (even less than 1% for the liquid phase) and less than 4 to 6% for the thermal diffusivity mixture data (or even less than 2% for the liquid phase up to a reduced temperature of about 0.98).

The results for the liquid kinematic viscosity and surface tension of R507 under saturation conditions obtained simultaneously from surface light scattering are summarized in Table V, where the quantity $\tilde{\nu}$ obtained for the viscosity directly from the experiment and the values from the literature used for data evaluation, as described below, are also listed. While a simple or modified Andrade-type equation may well represent the dynamic viscosity not too close to the critical point, and some authors have simply adopted this approach for the kinematic viscosity, this type of equation fails to represent the liquid kinematic viscosity reasonably for the

Table VI. Coefficients of Eq. (5) for R507

T range (K)	243–333
ν'_0	3.69455
ν'_1	-0.03365209
ν'_2	1.091591×10^{-4}
ν'_3	-1.222270×10^{-7}
rms (%)	0.52

Table VII. Coefficients of Eq. (6) for R507

T range (K)	243–T_C
σ_0	54.13
n	1.2773
rms (mN·m^{-1})	0.040

whole temperature range studied in the present investigation. Thus, we chose an empirical polynomial approach,

$$\nu' = \sum_{i=0}^{3} \nu'_i \left(\frac{T}{\mathrm{K}}\right)^i \qquad (\mathrm{mm^2 \cdot s^{-1}}) \tag{5}$$

to represent our experimental mixture viscosity data, where the coefficients for R507 are listed in Table VI. The standard deviations of our data relative to those calculated by Eq. (5) are also listed. The experimental data for the surface tension can be represented well by a van der Waals-type surface tension equation of the form

$$\sigma = \sigma_0 \left(1 - \frac{T}{T_C}\right)^n \qquad (\mathrm{mN \cdot m^{-1}}) \tag{6}$$

In Eq. (6), σ_0 and n are fit parameters, which are listed in Table VII for R507. The critical temperature was again adopted from our measurements; see above. The value determined from the fit for the exponent n is in good agreement with former investigations of pure refrigerants [24], where n varies between 1.20 and 1.26.

The results from surface light scattering are displayed in Figs. 4 and 5 for the kinematic viscosity and the surface tension of R507, respectively, again as functions of the reduced temperature. In addition to the mixture data, the pure-component data of R125 and R143a, which are reported separately in Ref. 25, are also shown in Figs. 4 and 5. The mixture results for the kinematic viscosity and surface tension also follow quite well a mass-weighted calculation scheme according to Eq. (4) using the pure-component values. For the measured viscosity of R507, excellent agreement with the predictions was observed as indicated in Fig. 4, where the standard deviation of our data relative to those calculated according to Eq. (4) is 0.63%. The mixture data for the surface tension of R507 displayed in Fig. 5 show a tendency toward a decreasing deviation from the prediction with decreasing distance from the critical point. These deviations from the prediction, however, are not larger than the measurement uncertainty, which is better than $\pm 0.2\,\mathrm{mN \cdot m^{-1}}$, being limited partly by the available density

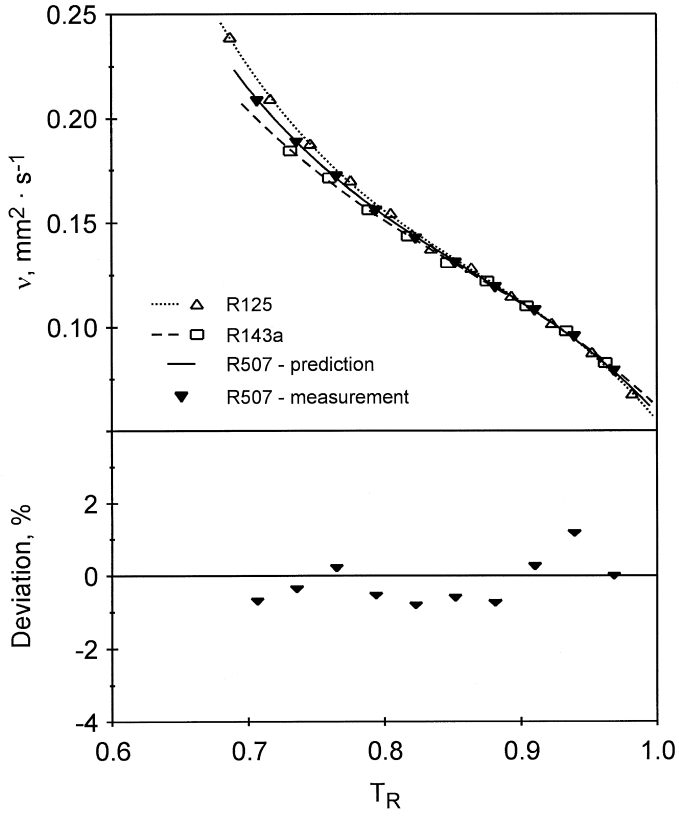

Fig. 4. Kinematic viscosity of the liquid phase under saturation conditions for the binary mixture R507 (▼) as a function of the reduced temperature in comparison to predictions (——) based on properties for the pure components R125 (·····△) and R143a (– –□).

data used for data evaluation. One must bear in mind that the quantity directly accessible in surface light scattering experiments is the ratio of the surface tension to the sum of the densities of the vapor and liquid phases. Thus, reliable reference data for the mixture densities under saturation conditions are needed, which were obtained with technical software from the manufacturer [26]. In a fashion similar to that for the measurement of the surface tension, the directly accessible quantity $\tilde{\nu}$ obtained for the viscosity is determined by both the vapor and the liquid properties, i.e.,

$$\tilde{\nu} = \frac{\eta' + \eta''}{\rho' + \rho''} \tag{7}$$

where η' and η'' are the dynamic viscosities of the liquid and vapor phases, respectively, and ρ' and ρ' are the densities of the liquid and vapor phases. If reliable reference data for vapor viscosities are not available, the approximation $\tilde{\nu} \approx \nu'$ can be used, which relies on the neglect of vapor properties compared with the respective liquid quantities and, thus, yields an approximate kinematic liquid viscosity ν'. An estimation based on reference data indicates that for the fluids under investigation this approximation results in a maximum systematic deviation from the true viscosity value of the liquid phase of about +4% for temperatures in the range $0.6 < T/T_C < 0.9$. For the highest temperatures studied in this work, the systematic error

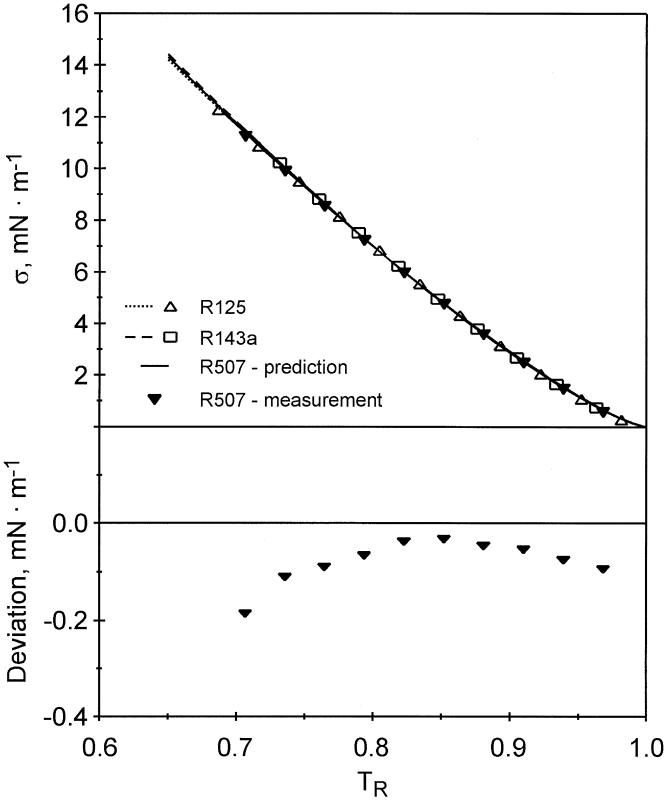

Fig. 5. Surface tension of the binary mixture R507 (▼) as a function of the reduced temperature in comparison to predictions (——) based on properties for the pure components R125 (·····△) and R143a (– –□).

caused by neglecting the influence of the vapor phase would decrease and vanish at the critical point. In the present work, however, data obtained for $\tilde{\nu}$ were combined with calculated data for the dynamic viscosity of the vapor phase [27] and density data for both phases [26] to get information on the liquid kinematic viscosity $\nu' = \eta'/\rho'$. Taking into account the uncertainties of the individual quantities entering into the calculation, the total uncertainty of our liquid kinematic viscosity data is estimated to be better than $\pm 2\%$, excluding the highest temperatures studied in this work ($T/T_C > 0.95$). A more detailed discussion regarding the accuracy achievable for surface tension and liquid kinematic viscosity from surface light scattering experiments is given in Refs. 25 and 28.

3.2. Ternary Mixture R404A

For the ternary mixture R404A ($T_C = 345.33$ K), the results obtained by light scattering from bulk fluids are summarized in Tables VIII and IX. Also for R404A, the thermal diffusivity and sound speed data can be well represented within experimental uncertainties by Eqs. (1) and (2), respectively, where the coefficients are given in Tables X and XI. The data of the thermal diffusivity and sound speed are presented as a function of the

Table VIII. Experimental Values of the Thermal Diffusivity a of R404A Under Saturation Conditions

Liquid phase		Vapor phase	
T (K)	a (10^{-8} m$^2 \cdot$ s^{-1})	T (K)	a (10^{-8} m$^2 \cdot$ s^{-1})
303.13	3.77	318.13	9.64
308.13	3.64	320.63	8.62
313.13	3.44	323.13	7.89
318.12	3.22	325.64	6.99
323.13	3.02	328.12	6.17
328.14	2.75	330.64	5.28
333.15	2.41	333.14	4.49
335.65	2.15	335.66	3.61
338.16	1.84	338.16	2.77
340.66	1.41	340.66	1.82
343.16	0.784	343.18	0.903
344.16	0.421	344.17	0.441

Table IX. Experimental Values of the Sound Speed c_s of R404A Under Saturation Conditions

Liquid phase		Vapor phase	
T (K)	c_s (m·s^{-1})	T (K)	c_s (m·s^{-1})
303.13	349.3	318.13	122.1
308.13	324.6	320.63	120.2
313.13	297.9	323.13	118.0
318.12	270.2	325.64	115.8
323.13	242.2	328.13	113.5
328.14	212.2	330.64	111.3
333.15	181.0	333.14	108.4
335.65	163.6	335.65	105.6
338.16	145.5	338.16	102.4
340.66	125.5	340.67	98.82
343.16	102.5	343.18	94.18
344.16	92.87	344.17	90.94

Table X. Coefficients of Eq. (1) for R404A

	Liquid phase	Vapor phase
T range (K)	303–344	318–344
a_0	240.4014	249.2255
a_1	−2.4347286	−1.2970941
a_2	7.336390×10^{-3}	1.663792×10^{-3}
a_3	-6.677883×10^{-6}	—
a_4	54.425	25.372
rms (%)	0.67	1.06

Table XI. Coefficients of Eq. (2) for R404A

	Liquid phase	Vapor phase
T range (K)	303–344	318–344
c_0	320.79	244.744
c_1	−0.7132	−0.48058
c_2	1166.58	65.220
φ	0.743	0.3013
rms (%)	0.25	0.12

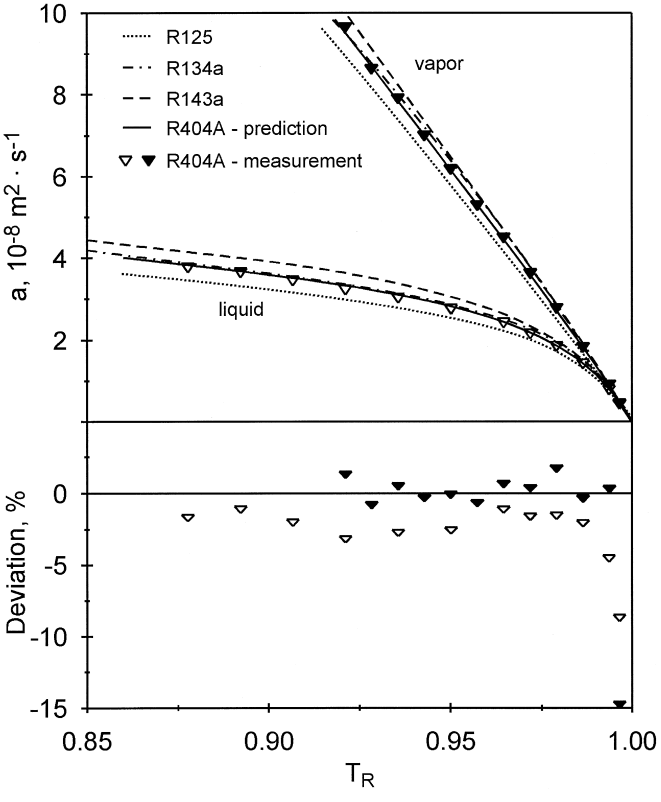

Fig. 6. Thermal diffusivity of the liquid (▽) and vapor (▼) phases under saturation conditions for the ternary mixture R404A as a function of the reduced temperature in comparison to predictions (——) based on properties for the pure components R125 (·····), R143a (– –), and R134a (–·–).

reduced temperature in Figs. 6 and 7, respectively. Here, in addition to data for R125 and R143a, data for R134a have to be taken into account in the correlation of the mixture data from those of the components. These data for R134a were taken from former measurements [29]. Again, the measured mixture data can best be correlated by the mass-weighted sum of the pure-component properties, as given by Eq. (4). From the deviation plots in Figs. 6 and 7, one observes that the deviation is again less than 1% for the sound speed and less than 5% for the thermal diffusivity for a reduced temperature up to 0.99.

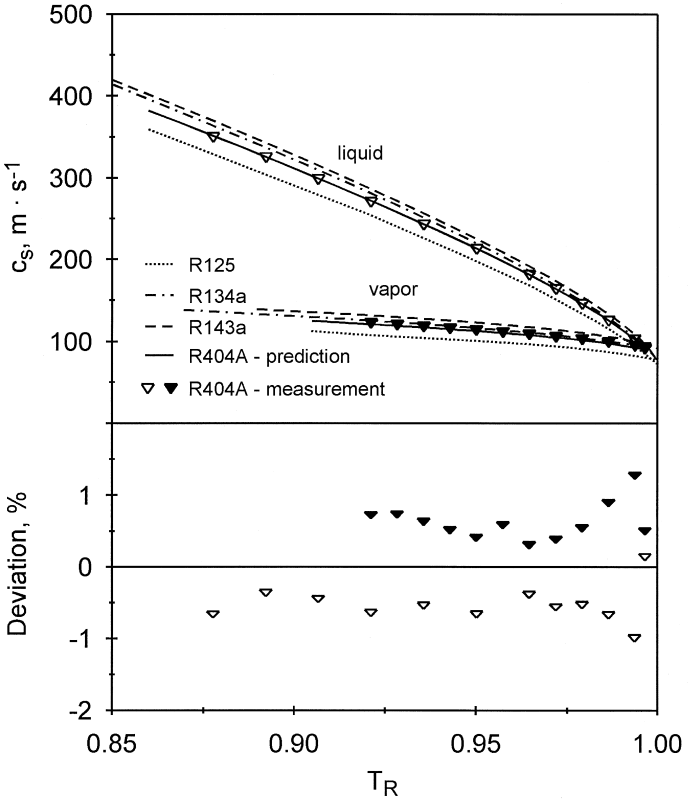

Fig. 7. Sound speed of the liquid (▽) and vapor (▼) phases under saturation conditions for the ternary mixture R404A as a function of the reduced temperature in comparison to predictions (——) based on properties for the pure components R125 (·····), R143a (– –), and R134a (–·–).

Table XII lists the results of the measurements of the liquid kinematic viscosity and surface tension of R404A under saturation conditions. For evaluation of the surface tension, the mixture densities are again calculated with technical software from the manufacturer [26]. Additionally, data for the dynamic viscosity of the saturated vapor of R404A were adopted from Ref. 27 to get information on the liquid kinematic viscosity. The data obtained from surface light scattering for the viscosity and surface tension of R404A have also been represented by Eqs. (5) and (6), respectively, where the coefficients are listed in Tables XIII and XIV. In Figs. 8 and 9, the measured data of the liquid kinematic viscosity and the surface tension,

Table XII. Viscosity and Surface Tension of R404A Under Saturation Conditions [a]

T (K)	$\tilde{\nu}$ ($mm^2 \cdot s^{-1}$)	η'' ($\mu Pa \cdot s$)	ρ' ($kg \cdot m^{-3}$)	ρ'' ($kg \cdot m^{-3}$)	ν' ($mm^2 \cdot s^{-1}$)	σ ($mN \cdot m^{-1}$)
243.15	0.2195	9.8	1256	11	0.2136	11.37
253.15	0.1985	10.1	1223	16	0.1927	10.04
263.15	0.1795	10.6	1188	22	0.1739	8.69
273.15	0.1639	11.1	1151	31	0.1587	7.40
283.15	0.1489	11.6	1111	42	0.1441	6.13
293.15	0.1362	12.1	1068	56	0.1320	4.90
303.15	0.1244	12.8	1020	76	0.1211	3.72
313.15	0.1121	13.6	966	101	0.1098	2.61
323.15	0.0994	14.7	901	137	0.0983	1.59
333.15	0.0823	16.4	816	192	0.0816	0.71

[a] Directly measured values for $\tilde{\nu}$ were combined with literature data for η'' from Ref. 27 and for ρ' and ρ'' from Ref. 26 to derive ν'. These density values were also used for the evaluation of σ.

Table XIII. Coefficients of Eq. (5) for R404A

T range (K)	243–333
ν'_0	3.98470
ν'_1	-0.03626960
ν'_2	1.169436×10^{-4}
ν'_3	-1.297730×10^{-7}
rms (%)	0.64

Table XIV. Coefficients of Eq. (6) for R404A

T range (K)	243–T_C
σ_0	53.54
n	1.2680
rms ($mN \cdot m^{-1}$)	0.039

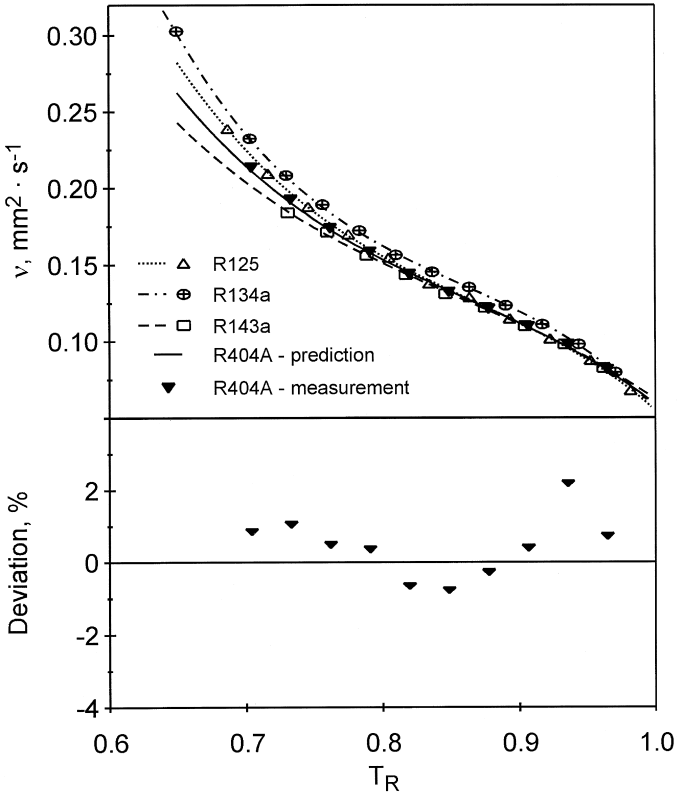

Fig. 8. Kinematic viscosity of the liquid phase under saturation conditions for the ternary mixture R404A (▼) as a function of the reduced temperature in comparison to predictions (——) based on properties for the pure components R125 (·····△), R143a (– –□), and R134a (–·–⊕).

respectively, of R404A are shown. The predictions given by Eq. (4) for both quantities of the mixture are indicated in the figures. Here, data for the surface tension and kinematic viscosity of R134a were taken into account from Ref. 25. As can be seen from the deviation plot in Fig. 8, the proposed correlation of the mixture viscosities from the pure-component data is in quite good agreement with the measured data for the entire temperature range in this work. For the surface tension of the ternary fluid mixture R404A, the same statements regarding the mixture rule as stated for the binary mixture are valid.

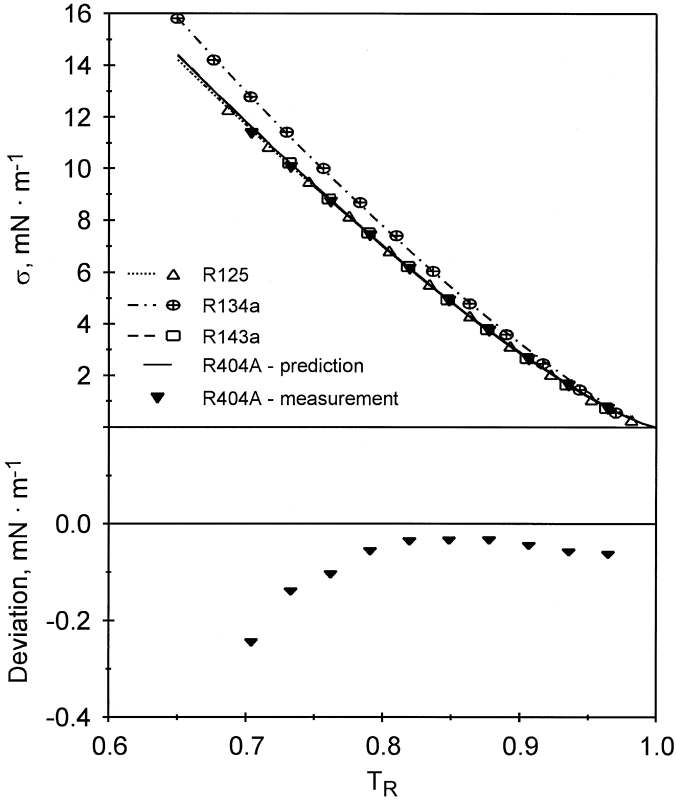

Fig. 9. Surface tension of the ternary fluid mixture R404A (▼) as a function of the reduced temperature in comparison to predictions (——) based on properties for the pure components R125 (·····△), R143a (– –□), and R134a (–·–⊕).

4. CONCLUSIONS

We have shown for the first time that the DLS technique can also be applied successfully to the investigation of ternary fluid mixtures. Several thermophysical properties have been measured for the ternary mixture R404A and also for the binary mixture R507, which contains two components of the ternary mixture R404. The experimental results suggest that the mixture data can best be represented by a mass-weighted sum of the pure-component data expressed as functions of the reduced temperature. This approach may also be useful for the prediction of properties of other mixtures.

ACKNOWLEDGMENTS

The investigated refrigerants were provided by Solvay Fluor und Derivate GmbH, Hannover. Parts of this work were supported by the Deutsche Forschungsgemeinschaft (DFG).

REFERENCES

1. J. N. Shaumeyer, R. W. Gammon, and J. V. Sengers, in *Measurement of the Transport Properties of Fluids*, W. A. Wakeham, A. Nagashima, and J. V. Sengers, eds. (Blackwell Scientific, Oxford, 1991), pp. 197–213.
2. A. Leipertz, *Int. J. Thermophys.* **9**:897 (1988); *J. Chem. Eng.* **34**:188 (1994); *Fluid Phase Equil.* **125**:219 (1996).
3. S. Will and A. Leipertz, in *Diffusion in Condensed Matter*, J. Kärger, P. Heitjans, and R. Haberlandt, eds. (Vieweg, Wiesbaden, 1999), pp. 219–244.
4. A. P. Fröba, S. Will, and A. Leipertz, *Fluid Phase Equil.* **161**:337 (1999).
5. M. Corti and V. Degiorgio, *J. Phys. C Solid State Phys.* **8**:953 (1975).
6. M. Hendrix, A. Leipertz, M. Fiebig, and G. Simonsohn, *Int. J. Heat Mass Transfer* **30**:333 (1987).
7. S. Will, A. P. Fröba, and A. Leipertz, *Int. J. Thermophys.* **19**:403 (1998).
8. E. Gulari, R. J. Brown, and C. J. Pings, *AIChE J.* **19**:1196 (1973).
9. G. Wu, M. Fiebig, and A. Leipertz, *Int. J. Heat Mass Transfer* **31**:1471 (1988); **31**:2555 (1988).
10. H.-W. Fiedel, G. Schweiger, and K. Lucas, *J. Chem. Eng. Data* **36**:169 (1991).
11. G. Simonsohn, *Opt. Acta* **30**:875 (1983).
12. A. Leipertz, K. Kraft, and G. Simonsohn, *Fluid Phase Equil.* **79**:201 (1992).
13. K. Kraft and A. Leipertz, *Int. J. Thermophys.* **16**:445 (1995).
14. A. P. Fröba, S. Will, and A. Leipertz, *Appl. Opt.* **36**:7615 (1997).
15. S. Will and A. Leipertz, *Int. J. Thermophys.* **18**:1339 (1997).
16. S. Will and A. Leipertz, *Int. J. Thermophys.* **20**:791 (1999).
17. B. J. Ackerson and H. J. M. Hanley, *J. Chem. Phys.* **73**:3568 (1980).
18. J. W. Schmidt and M. R. Moldover, *J. Chem. Eng. Data* **39**:39 (1994).
19. J. W. Schmidt, E. Carrillo-Nava, and M. R. Moldover, *Fluid Phase Equil.* **122**:187 (1996).
20. J. Yata, M. Hori, and T. Minamiyama, in *Proc. Jap. Symp. Thermophys. Prop. 11/1990* (1990), pp. 111–114.
21. D. Langewin, *Light Scattering by Liquid Surfaces and Complementary Techniques* (Marcel Dekker, New York, 1992).
22. K. Kraft and A. Leipertz, *Int. J. Thermophys.* **15**:387 (1994).
23. A. P. Fröba, S. Will, and A. Leipertz, *Int. J. Thermophys.* **22**:1021 (2001).
24. M. Okada and Y. Higashi, *Proceedings International Conference CFCs, the Day After* (Padova, 1994), pp. 541–548.
25. A. P. Fröba, S. Will, and A. Leipertz, *Int. J. Thermophys.* **21**:1225 (2000).
26. Solvay Fluor & Derivate, SOLKANE Refrigerant Software, Version 2.0 (1999).
27. National Institute of Standard and Technology (NIST), *Standard Reference Database 14, Version 4* (2000).
28. A. P. Fröba and A. Leipertz, *Int. J. Thermophys.* **22**:41 (2001).
29. K. Kraft and A. Leipertz, *Fluid Phase Equil.* **125**:245 (1996).